Applied Catalysis B: Environmental 100 (2010) 97–101

Contents lists available at ScienceDirect

Applied Catalysis B: Environmental

journal homepage: www.elsevier.com/locate/apcatb

Hybrid Bi_2SiO_5 mesoporous microspheres with light response for environment decontamination

Ling Zhang, Wenzhong Wang*, Songmei Sun, Jiehui Xu, Meng Shang, Jia Ren

State Key Laboratory of High Performance Ceramics and Superfine Microstructures, Shanghai Institute of Ceramics, Chinese Academy of Sciences, 1295 Dingxi Road, Shanghai 200050, PR China

ARTICLE INFO

Article history:
Received 12 April 2010
Received in revised form 13 July 2010
Accepted 15 July 2010
Available online 23 July 2010

Keywords:
Mesostructure
Bi_2SiO_5
Photocatalyst
Periodic mesoporous organosilicas

ABSTRACT

A hybrid mesostructured photocatalyst prepared by using the "postsynthetic modification" approach with the periodic mesoporous organosilicas (PMO) framework and bismuth nitrate was studied. The morphology and structure of the hybrid Bi_2SiO_5 photocatalyst were characterized by X-ray diffraction (XRD), transmission electron microscopy (TEM) and N_2 adsorption–desorption isotherms. These results of characterization show that the as-prepared Bi_2SiO_5 keeps a semi-ordered mesostructure as the PMO framework. The results of density functional theory calculations indicated that the conduction band bottom of Bi_2SiO_5 mainly consist of Bi 6s orbits and O 2p, O 2s, while the valence band top mainly consist of Si 3p, O 2p, and Bi 5d orbits. The as-prepared Bi_2SiO_5 exhibited efficient photocatalytic activity in the decomposition of a widely used dye, tetraethylated rhodamine (RhB), and phenol in water under the simulative sunlight irradiation. Further, the photocatalytic experiment results show that the hybrid Bi_2SiO_5 synthesized based on PMO was more efficient than the pure mesoporous Bi_2SiO_5 in decomposing the organic pollutant, which means the hybrid organic groups dispersed in the PMO framework is advantageous to improve the efficiency of the photocatalyst.

1. Introduction

During the last decade, photocatalytic technology for water decontamination has received great attentions due to its mild reaction conditions and no secondary pollutant [1–3]. The semiconductor photocatalysts with various morphologies, microstructures [4–8], and components [9,10] have been developed up to now. Among these materials, mesostructured photocatalysts are highly desirable because of their distinct characteristics including large surface area and inner connected channels [11,12]. Large surface area can supply more active sites and adsorb more pollutant. On the other hand, the inner connected channels facilitate the access of reactant molecules to active sites and also improve the distribution of photon energy over the porous frameworks. Consequently, the mass transfer and light utilization efficiency of heterogeneous systems in photocatalytic reactions can be enhanced.

Porous TiO_2 is the most studied mesoporous semiconductor photocatalyst. It had been prepared by various methods, typically involving of organic soft template or nanocasting technology [9,10]. However, the fabrication of mesostructured titania with ordered crystalline frameworks remains a great challenge. The inherent reason for this challenge is attributed to the fact that the mesoporous framework of TiO_2 easily collapse during thermal treatment, which is indispensable for removing the organic soft template and enhancing the crystallization of the TiO_2 framework. In addition, the high temperature treatment is also a prevalent method to eliminate the remnant pollutant in the pore channels for recovering its photocatalytic activity [13]. Therefore, the creative design of a new mesostructured semiconductor photocatalyst with high thermal stability is desirable.

Recently, periodic mesoporous organosilicas (PMO) obtained through the coupling of inorganic and organic components are particularly attractive due to their combination of the properties of organic and inorganic building blocks within a single material. The possibility to combine the enormous functional variation of organic chemistry with the advantages of a thermally stable and designable inorganic substrate made PMO promising for numerous applications, including optical and catalytic systems [14]. Herein, we reported a simple and versatile strategy that has allowed us to design and synthesize alternative mesostructured photocatalysts to TiO_2. PMO hollow spheres were applied as "frame" but not merely a template to synthesis the mesoporous bismuth silicate (Bi_2SiO_5) photocatalyst by a "postsynthetic modification" method. Bi_2SiO_5 has been reported as a catalyst for the oxidation coupling of methane [15,16]. In this work, the Bi ions were directly introduced into the PMO framework by sintering the $Bi(NO_3)_3$ with the PMO microspheres in air and thus crystalline Bi_2SiO_5 formed. The resulting hybrid mesostructured Bi_2SiO_5, possess the advantages of

* Corresponding author. Tel.: +86 21 5241 5295; fax: +86 21 5241 3122.
E-mail address: wzwang@mail.sic.ac.cn (W. Wang).

0926-3373/$ – see front matter © 2010 Elsevier B.V. All rights reserved.
doi:10.1016/j.apcatb.2010.07.018

the PMO materials: thermal–mechanic stability [17] and uniform distribution of functional organic groups inside the pore wall. The latter character of the PMO materials is favorable for the transporting of the carrier-charges comparing with the pure silica [18,19]. These favorable textural properties, combining with increased surface reaction cites and mass transfer, are advantageous to yield a highly efficient photocatalytic reaction for environmental decontamination. To the best of our knowledge, it is the first example of the preparation of mesostructured photocatalyst with the PMO frameworks.

2. Experimental

2.1. Synthesis of hybrid Bi_2SiO_5 mesoporous microsphere

0.50 g of FC-4 ($C_3F_7O(CFCF_3CF_2O)_2CFCF_3CONH(CH_2)_3N^+(C_2H_5)_2CH_3I^-$)was dissolved in 95 ml of water and stirred at room temperature for 1 h before the addition of 0.20 g of CTAB and 0.7 ml NaOH (2 M). Then, the mixture solution was heated to 80 °C. BTME (1,2-bis(trimethoxysilyl)ethane, 0.65 ml, Aldrich, 96%) was introduced under vigorous stirring. After 2 h, the white product was collected by filtration and dried at room temperature. To remove the surfactant, the above as-synthesized samples were refluxed in ethanol for 8 h at 60 °C.

Bismuth nitrate ($Bi(NO_3)_3{\cdot}5H_2O$) and above PMO powder in stoichiometric proportions (0.3:1 molar ratio) were mixed and ground. The mixture powder was calcined at 300 °C for 3 h in air. The white powders were obtained after they were cooled down to room temperature.

2.2. Synthesis of mesoporous Bi_2SiO_5 microsphere

In a typical synthesis of IBN-4 mesoporous spheres, 0.25 g of Pluronic P123 and 0.7 g of FC-4 were dissolved in 40 ml of HCl solution (0.02 M), followed by the introduction of 1.0 g of TEOS. The solution was stirred at 30 °C for 20 h and then transferred into an autoclave at 100 °C for 1 day. The white product was collected by filtration and dried at room temperature. To remove the surfactant, the above as-synthesized samples were refluxed in ethanol for 8 h at 60 °C.

Bismuth nitrate ($Bi(NO_3)_3{\cdot}5H_2O$) and above IBN-4 powder in stoichiometric proportions (0.3:1 molar ratio) were mixed and ground. The mixture powder was calcined at 300 °C for 3 h in air. The white powders were obtained after they were cooled down to room temperature.

2.3. Characterization methods

Powder XRD patterns were collected on a Rigaku D/MAX-2550 V diffractometer at 30 kV and 15 mA (Co K*a* radiation). TEM analysis was performed using a JEOL 2100F electron microscope operated at 200 kV. N_2 adsorption–desorption isotherms were obtained using a Micromeritics Tristar 3000 pore analyzer at 77 K. BET and BJH analyses were used to determine the surface area, pore size, and pore volume.

The UV–vis absorption spectra were measured on a UV–vis spectrophotometer (Hitachi 3010). The photocatalytic activity of the Bi_2SiO_5 nanoparticles for decomposition of (RhB) and phenol were evaluated under irradiation of a 500 W Xe lamp at the natural pH value. The initial concentration of RhB and phenol was 10^{-5} mol l^{-1} and 20 mg/l, respectively, with a catalyst loading of 1.0 g/l. As a comparison, commercial P25 powders were used as photocatalysts for the photocatalytic tests. After the elapse of definite time, a small quantity of the solution was taken, and the concentrations of pollutants were determined by using a UV–vis spectrophotometer. Each time before the absorption measurement, the sample solution was centrifuged at 5000 rpm min^{-1} for 10 min in order to separate the catalyst particles from the solution. The absorption was converted to the pollutants concentration referring to a standard curve showing a linear behavior between the concentration and the absorption at the special wavelengths.

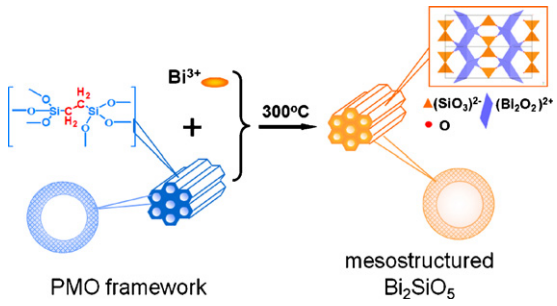

Scheme 1. Synthesis of mesostructured Bi_2SiO_5 by Bi ions and PMO framework.

3. Results and discussion

3.1. Synthesis and characterization of hybrid Bi_2SiO_5 mesoporous microsphere

The synthesis of hybrid Bi_2SiO_5 mesoporous microsphere (HBSO-MM) was carried out via two stages as shown in Scheme 1: (a) the preparation of PMO hollow spheres (PMO-HM) according to the Ref. [20]. An 1,2-bis(trimethoxysilyl)ethane (BTME) was employed as the hybrid silica precursor to synthesize the PMO-HM, with ethane groups in the framework; (b) the formation of the HBSO-MM by sintering the $Bi(NO_3)_3$ powder with the PMO-HM in air. The morphology and mesoporous characters of the PMO-HM and HBSO-MM were observed by transmission electronic microscopy (TEM). In Fig. 1a, the diameter of hollow core in the PMO-HM was about 120 nm and the thickness of the mesostructured shell was about 30 nm. For the HBSO-MM, mesoporous

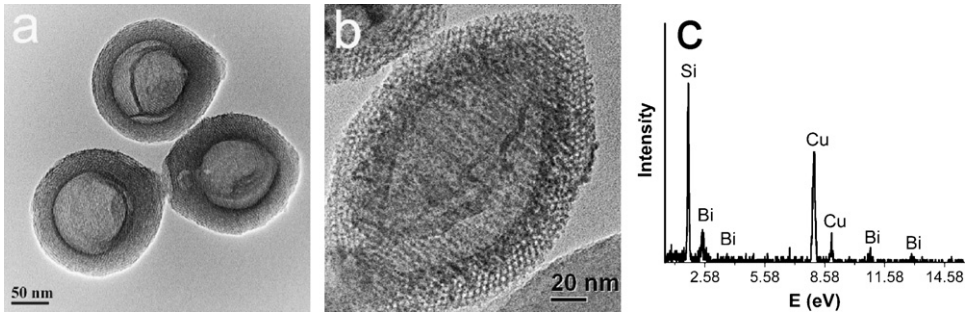

Fig. 1. (a) TEM image of PMO-HM; (b) high-magnification TEM image of HBSO-MM; (c) EDX spectrum of the HBSO-MM, taken from the area shown in (b).

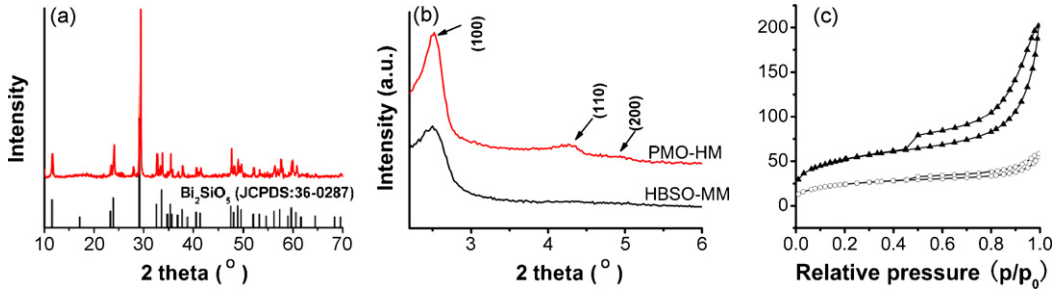

Fig. 2. (a) XRD pattern of HBSO-MM in the high-angle range; (b) XRD patterns of PMO-HM and HBSO-MM in the low-angle range; (c) N_2 adsorption–desorption isotherms of PMO-HM (▲) and HBSO-MM (◯).

channel in the shell and the hollow cavity can be also clearly observed and the mesopore size is estimated to be ~3.0 nm, as shown in Fig. 1b (more spheres shown in Fig. S1). The EDX spectrum result shown in Fig. 1c proves the Bi ions were introduced into the mesoporous framework. The above evidences suggest that the Bi ions were successfully introduced into the PMO-HM framework.

The XRD patterns of the samples were obtained in different scan range. In Fig. 2a, it can be seen that all observable peaks are indexed to a pure orthorhombic Bi_2SiO_5 phase (JCPDS: 36-0287) and no other peaks were detected. It means that highly pure and crystalline Bi_2SiO_5 were formed by sintering the $Bi(NO_3)_3$ powder with the PMO-HM. The $(Bi_2O_2)^{2+}$ layers are formed of slightly distorted squared oxygen planes and inserted parallel to the corner-sharing $(SiO_3)^{2-}$ tetrahedron in columns of PMO. As a result, the two-dimensional structure of Bi_2SiO_5 was built up from an intergrowth of $(SiO_3)^{2-}$ pyroxene file layers inserted between $(Bi_2O_2)^{2+}$ layers. These squares are capped alternatively above and below by the bismuth atoms (as shown in Scheme 1). The mesostructure inside the shells of PMO-HM and HBSO-MM were confirmed by the XRD patterns at low-angle scale (Fig. 2b). The XRD pattern of PMO-HM exhibited three definite peaks indexed to (1 0 0), (1 1 0), (2 0 0) indicates a highly ordered 2D mesostructure with typical hexagonal pattern *P6m* symmetry, whereas the XRD pattern of HBSO-MM only keeps one peak of (1 0 0). It implies the HBSO-MM partly maintained the ordered mesostructure, though a few of pores near the hollow core were over filled. The $(Bi_2O_2)^{2+}$ layers alternately inserted into the $(SiO_3)^{2-}$ pyroxene file layers could not destroy the ordered mesostructure of the PMO-HM totally.

The N_2 adsorption–desorption isotherms for the PMO-HM and HBSO-MM are shown in Fig. 2c. The typical IV isotherm indicates that both samples possess the mesoporous structures. The H4 loop with parallel branches at relative pressures between 0.45 and 1.0 is attributed to the hollow cavity space [21]. Remarkably, the cumulative amount of adsorption/desorption N_2 in the HBSO-MM was reduced comparing with the PMO-HM sample. The average mesopore diameter of PMO-HM and HBSO-MM calculated by the Barrett–Joyner–Halenda (BJH) model was 5.1 nm and 3.3 nm, respectively. Accordingly, the Brunauer–Emmett–Teller (BET) surface area, pore volume of PMO-HM and HBSO-MM were reduced from 186.4 $m^2\,g^{-1}$ and 0.238 $cm^3\,g^{-1}$ to 88.6 $m^2\,g^{-1}$ and 0.078 $cm^3\,g^{-1}$, respectively. The difference between the two samples would be explained by the crystallinity and pores size. First, the size of crystal lattice of Bi_2SiO_5 was bigger than that of SiO_2. When the Bi ions entered the mesoporous framework, the wall thickness would increase resulting in the reduction of pore size. Second, highly crystallinity of HBSO-MM samples resulted to reduce mesoporous surface roughness and thus to reduce the surface areas [22]. In addition, the density of bulk Bi_2SiO_5 (7.87 $g\,cm^{-3}$) is higher than that of bulk silica (2.26 $g\,cm^{-3}$) which must also be taken into account.

As control, bismuth nitrate and PMO-HM with different proportions were mixed and sintered at 300 °C. When the molar ratio of $Bi(NO_3)_3$ to PMO was doubled, the pores and cavity of the PMO-M would be mostly filled. The responding XRD pattern shows that Bi_2SiO_5 and Bi_2O_3 mixture were formed (more detail see in Fig. S2). In addition, Bi_2O_x and SiO_2 mixtures but not Bi_2SiO_5 were synthesized if SiO_2 nanospheres were utilized as silica framework under the same experimental conditions as described above. Taken account of the above results, the mesopores in the framework is very important for the formation of pure Bi_2SiO_5. Generally, metal nitrate is not stable with the heat treatment. $Bi(NO_3)_3$, with a low melt point (30 °C), would be decomposed to BiO_x, NO_2, and O_2 under heat treatment. The melted Bi ions could diffuse through the mesoporous channels by the capillary force and then react with $(SiO_3)^{2-}$ tetrahedral units to form Bi_2SiO_5 at high temperature. When the concentration of Bi precursor increased, differences in the concentration of precursor between the hollow core and the mesopores would provide the driving force to accelerate the diffusion of precursor from the mesochannel to the inner core. So, Bi_2O_3 was formed in the inner core by the superfluous precursor decomposition. This process was different from the synthesis of inorganic oxide/SiO_2 mesoporous spheres by the infiltration process in the solution [23–25]. In that case, once the inorganic precursor solution is introduced, they prefer to aggregate in the hollow cores rather than to be isolated in mesopores in order to reduce the surface energy.

3.2. Electric structure and photocatalytic performance

Fig. S3 shows the UV–vis diffuse reflectance spectra of the as-synthesized HBSO-MM. The wavelength at the absorption edge, λ, is determined as the intercept on the wavelength axis for a tangent line drawn on absorption spectra. The absorption for the sample locates at ca. 405 nm. The band gap energy (E_g) calculated on the basis of the corresponding absorption edges is 3.29 eV. Ab initio calculations were also performed to evaluate the electronic structures of Bi_2SiO_5. Fig. 3a and b shows the densities of states and band structures of Bi_2SiO_5 calculated by VASP. The lowest unoccupied state and the highest occupied state are at the Γ point as shown in Fig. 3a. This means that Bi_2SiO_5 is a direct gap semiconductor, allowing the direct transition from Γ to Γ. The band gap of Bi_2SiO_5 was estimated to be 2.92 eV. Generally, the band gap calculated by DFT is smaller than that obtained experimentally, which is frequently pointed out as a common feature of DFT calculations [26]. Fig. 3b shows the partial and total densities of states of Bi_2SiO_5. It is clear that the conduction band bottom mainly consists of Bi 6s orbits and O 2p, O 2s, while the valence band top mainly consists of Si 3p, O 2p, and Bi 5d orbits. Compared with Bi_2O_3, of which the valence band top consists of Bi 6s and O 2p orbits [27], the valence band of Bi_2SiO_5 is more localized. It suggests that the photo-generated holes in Bi_2SiO_5 have more effective paths.

To check the real photocatalytic properties, firstly, RhB (rhodamine B) dye was selected because it is convenient to observe the decoloration process. In Fig. 4a, a fast decrease of RhB absorp-

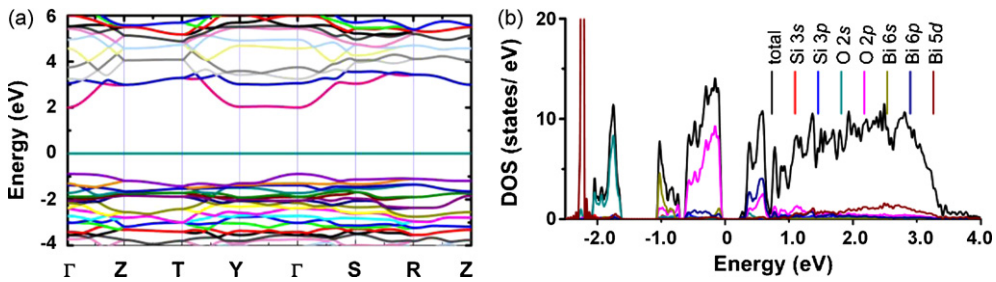

Fig. 3. (a) Calculated band structures for Bi_2SiO_5 by GGA along the high-symmetry axes of the Brillouin zone; (b) total DOS and partial DOS of Bi_2SiO_5 obtained by GGA.

tion at the wavelength of 553 nm is observed after the HBSO-MM powder was added into the dye solution. Nearly 60% of RhB in the solution were absorbed by the HBSO-MM in 15 min. However, no apparent absorption increase was observed when the time increase to 30 min, even to 60 min. Fig. 4b displays the temporal evolution of the spectra during the photodegradation of RhB mediated by the HBSO-MM sample. Under Xe light illumination, the spectral maximum rapidly shifted from 553 nm to 500 nm and decreased to zero within 40 min. The sharp decrease and shift of the major absorption band of RhB indicate that the HBSO-MM sample has excellent absorptive ability and photocatalytic activity. Especially, the fast adsorption of dyes in the porous channels of the HBSO-MM was a crucial step for efficiently decomposing the pollutant in the photocatalytic reaction.

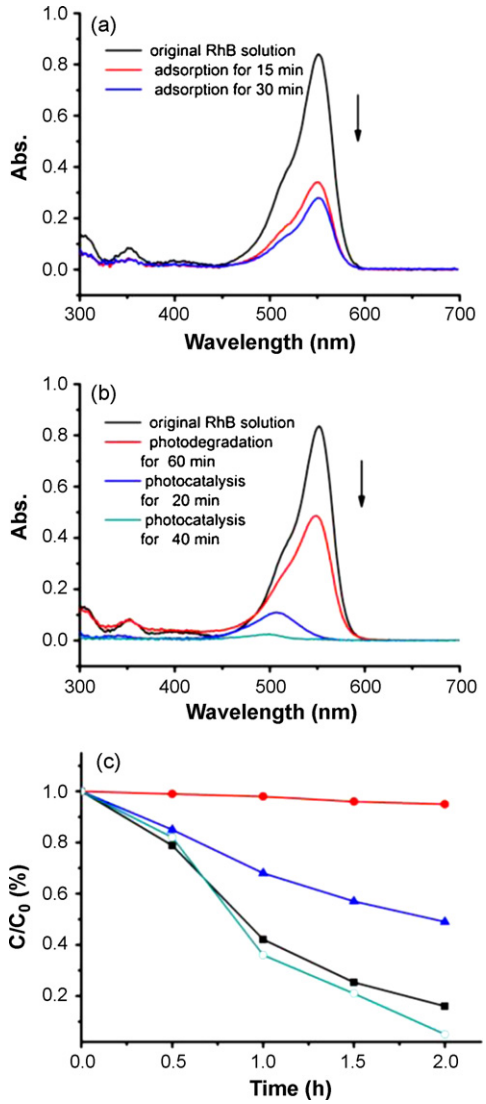

Fig. 4. UV–visible spectral changes of RhB (1×10^{-5} M) in an aqueous HBSO-MM solution as a function of (a) absorption time and (b) irradiation time (catalyst, 0.1 g l^{-1}); (c) photocatalytic degradation of phenol under different conditions: (●) without photocatalyst, (▲) with mesoporous Bi_2SiO_5, (■) with HBSO-MM, and (○) with P25 as photocatalyst.

In order to eliminate the photosensitization in the RhB photocatalytic decomposition process, colorless phenol was selected as a model pollutant. Fig. 4b shows the photodegradation efficiencies of phenol as a function of irradiation time under different conditions. The different decreases of the concentration of phenol were observed with the increase of the irradiation time in presence of three photocatalysts. Clearly, more than ninety percent of phenol was degraded in 2 h under the irradiation of Xe over the HBSO-MM and P25 powders. The HBSO-MM catalyst's performance was nearly comparable to the commercial P25 powders, but the size of latter catalyst was too small to separate from the aqueous reaction system which limits its practical application. Meanwhile, no degradation of phenol was observed without the photocatalyst. The same photocatalytic reaction was performed over the Bi_2SiO_5 mesoporous microspheres (the relative synthesis and morphology are shown in supporting information) to distinguish the role of the organic ethane groups in the HBSO-MM. The photocatalytic experiments results show that it has weaker decomposing ability for the phenol solutions comparing with the HBSO-MM sample. The above results prove that the Bi_2SiO_5 has photocatalytic oxidation ability to decompose the organic pollutant. Furthermore, it seems rational that the CH_2–CH_2 groups distributed in the mesostructured framework were advantageous for improving the photocatalytic efficiency because the organic group generally has lower Fermi level than the pure silica, which is favorable to transport the carrier-charges in the photocatalyst.

For actual application, the stability of a photocatalyst is first to be considered. The photocatalytic stability of the as-synthesized HBSO-MM powders was confirmed by repeating the decomposition and heat treatment processes to recover its activity for five times. The recycle experiments show that the HBSO-MM could still decompose the RhB dye completely in the same irradiation time (as shown in Fig. S4). And the sample could keep the mesostructure after the recycle experiments (as shown in Fig. S6).

4. Conclusion

In summary, we have demonstrated a "postsynthetic modification" approach with the PMO framework to fabricate a hybrid mesostructured Bi_2SiO_5 hollow microsphere. Taking the advantage of the thermal stability and the inner connected channel of the PMO framework, the Bi ions could easily diffuse into the channels of the shell and directly react with the silica to form Bi_2SiO_5 at high temperature. Controlling a proper ratio of Bi precursor to the PMO, the Bi_2SiO_5 formed in situ the mesoporous wall of the PMO-HM but not Bi_2O_3 formed in the hollow core. The $(Bi_2O_2)^{2+}$ layers could alter-

nately insert into the $(SiO_3)^{2-}$ tetrahedral units and partly keep the ordered mesoporous structure. The photocatalytic experiment results show that the HBSO-MM synthesized based on PMO was more efficient than the mesoporous Bi_2SiO_5 for decomposing the organic pollutant, which means the organic groups dispersed in the PMO framework is advantageous to improve the efficiency of the photocatalyst. The methodology reported herein is versatile and convenient and can be extended to a broad range of framework and guest species due to the structural diversity of the PMO framework and silicate. Based on such a unique architecture, these composites are expected to be used in a wide range of applications as a novel "microreactors" such as high-performance catalysis and energy conversion materials. Especially, it is promising to improve the photocatalytic activity by inducing various aromatic and π-conjugated bridging organic groups into the PMO framework.

Acknowledgements

This work was supported by the National Natural Science Foundation of China (Grant Nos. 50972155 and 50902144) and the National Basic Research Program of China (973 Program, 2007CB613302).

Appendix A. Supplementary data

Supplementary data associated with this article can be found, in the online version, at doi:10.1016/j.apcatb.2010.07.018.

References

[1] S.B. Wang, H.M. Ang, M.O. Tade, Environ. Int. 33 (2007) 694–705.
[2] O.K. Dalrymple, D.H. Yeh, M.A. Trotz, J. Chem. Technol. 82 (2007) 121–134.
[3] F. Al Momani, N. Jarrah, Environ. Technol. 30 (2009) 1085–1093.
[4] H.T. Yu, X. Quan, Prog. Chem. 21 (2009) 406–419.
[5] H.A.J.L. Mourao, V.R. de Mendonca, A.R. Malagutti, C. Ribeiro, Quim. Nova 32 (2009) 2181–2190.
[6] D.G. Shchukin, D.V. Sviridov, J. Photochem. Photobiol. C 7 (2006) 23–39.
[7] Q. Dong, H.L. Su, W. Cao, J. Solid State Chem. 180 (2007) 949–955.
[8] J.G. Yu, Y.R. Su, B. Cheng, Adv. Funct. Mater. 17 (2007) 1984–1990.
[9] X.F. Chen, X.C. Wang, X.Z. Fu, Energy Environ. Sci. 2 (2009) 872–877.
[10] Q. Yuan, Y. Liu, L.L. Li, Z.X. Li, C.J. Fang, W.T. Duan, X.G. Li, C.H. Yan, Micropor. Mesopor. Mater. 124 (2009) 169–178.
[11] G.S. Li, D.Q. Zhang, J.C. Yu, Chem. Mater. 20 (2008) 3983–3992.
[12] Y. Shioya, K. Ikeue, M. Ogawa, M. Anpoa, Appl. Catal. A: Gen. 254 (2003) 251–259.
[13] X.C. Wang, J.C. Yu, C. Ho, Y.D. Hou, X.Z. Fu, Langmuir 21 (2005) 2552–2559.
[14] F. Hoffmann, M. Cornelius, J. Morell, M. Froba, Angew. Chem. Int. Ed. 45 (2006) 3216–3251.
[15] E.N. Voskresenkaya, L.I. Kurteeva, V.P. Zhereb, A.G. Anshits, Catal. Today 13 (1992) 599–602.
[16] R.G. Chen, J.H. Bi, L. Wu, W.J. Wang, Z.H. Li, X.Z. Fu, Inorg. Chem. 48 (2009) 9072–9076.
[17] Y.D. Xia, W.X. Wang, R. Mokaya, J. Am. Chem. Soc. 127 (2005) 790–798.
[18] N. Mizoshita, M. Ikai, T. Tani, S. Inagaki, J. Am. Chem. Soc. 131 (2009) 14225–14227.
[19] M.A. Wahab, S. Sudhakar, E. Yeo, A. Sellinger, Chem. Mater. 20 (2008) 1855–1861.
[20] L. Zhang, S.Z. Qiao, Y.G. Jin, Z.G. Chen, H.C. Gu, G.Q. Lu, Adv. Mater. 20 (2008) 805–809.
[21] P.J. Kooyman, M.J. Verhoef, E. Prouzet, Stud. Surf. Sci. Catal. 129 (2000) 535–542.
[22] X.Y. Lai, X.T. Li, W.C. Geng, J.C. Tu, J.X. Li, S.L. Qiu, Angew. Chem. Int. Ed. 46 (2007) 738–741.
[23] Y. Yamada, M. Mizutani, T. Nakamura, K. Yano, Chem. Mater. 22 (2010) 1695–1703.
[24] L. Li, J. Ding, J.M. Xue, Chem. Mater. 21 (2009) 3629–3637.
[25] G.L. Li, E.T. Kang, K.G. Neoh, X.L. Yang, Langmuir 25 (2009) 4361–4364.
[26] A. Kudo, H. Kato, S. Nakagawa, J. Phys. Chem. B 104 (2000) 571–575.
[27] L.S. Zhang, W.Z. Wang, J. Yang, Z. Chen, W.Q. Zhang, L. Zhou, S. Liu, Appl. Catal. A 308 (2006) 105–110.